

Crystallography-Induced Correlations in Pore Ordering of Anodic Alumina Films

Ilya V. Roslyakov,^{†,‡} Dmitry S. Koshkodaev,[§] Andrei A. Eliseev,^{†,‡} Daniel Hermida-Merino,^{||}
Andrei V. Petukhov,^{⊥,#} and Kirill S. Napolskii^{*,†,‡}

[†]Department of Chemistry and [‡]Department of Materials Science, Lomonosov Moscow State University, Moscow 119991, Russia

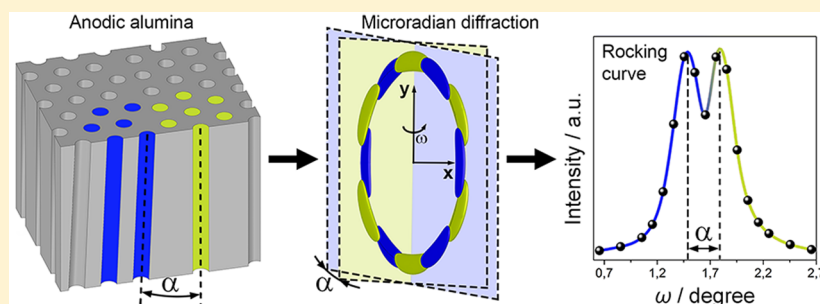
[§]National Research University of Electronic Technology, Zelenograd, Moscow 124498, Russia

^{||}DUBBLE CRG ESRF BM26, F-38043 Grenoble Cedex, France

[⊥]van 't Hoff Laboratory for Physical and Colloid Chemistry, Debye Institute for Nanomaterials Science, Utrecht University, 3508 TB Utrecht, The Netherlands

[#]Laboratory of Physical Chemistry, Department of Chemical Engineering and Chemistry, Eindhoven University of Technology, Eindhoven 5600 MB, The Netherlands

Supporting Information



ABSTRACT: A crystallographic approach to tailoring the morphology and ordering degree of the porous structure of alumina films obtained by anodization of single-crystalline aluminum is discussed. The examination of porous structure of anodic alumina films formed on low-index and vicinal planes of Al single crystals under self-ordering conditions by high-resolution small-angle X-ray scattering revealed the existence of two pore growth directions on vicinal facets. The inclination of channels from the normal to the metal surface is explained by the competitive impact of electromigration driving force and the crystallographic anisotropy of the substrate. It was also shown that pores growing in different directions during anodization retain hexagonal domains with various in-plane orientations. These results for the first time demonstrate the strong correlations between the longitudinal alignment and in-plane packing options of pores in anodic alumina films.

INTRODUCTION

Anodization is a widespread technological process that allows one to produce oxide films with various composition and morphology. Nowadays, anodic oxide layers on aluminum,^{1–3} titanium,^{4–7} zirconium,^{8,9} tungsten,^{6,10} and other valve metals are routinely prepared and widely used owing to their unique physicochemical properties. Among those materials, the unique property of anodic aluminum oxide (AAO) is the possibility to obtain honeycomb-like porous structure with highly ordered vertical cylindrical channels. Such morphology of the porous anodic alumina formed under certain conditions allows achieving extremely high density of pores (ca. 10^{10} to 10^{11} cm⁻²) and narrow pore size distribution that offers great opportunities for the creation of various nanostructured functional materials. In particular, large-scale photonic¹¹ and plasmonic¹² crystals for manipulation of light, highly permeable membranes for gas and liquid separation,^{13–15} and templates

for synthesis of ordered arrays of high-aspect-ratio nanostructures^{16–18} are commonly prepared using anodic alumina films.

The degree of pore ordering in AAO film can be described by three major order parameters: (i) Transverse (in-plane) positional order correlates to the dispersion of interpore distances; (ii) transverse orientational order is related to the preservation of the in-plane orientations of the hexagons formed by neighboring channels; and (iii) longitudinal (out-of-plane) orientational order defines how well the direction of pore growth is maintained across the film.

Various experimental conditions, such as voltage, temperature, electrolyte composition, and anodization duration, have been empirically varied to improve these order parameters.¹⁹ Recently the influence of the microstructure of the aluminum

Received: May 25, 2016

Revised: August 9, 2016

Published: August 10, 2016



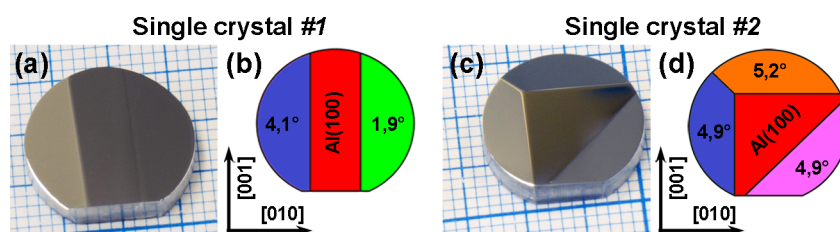


Figure 1. Photos (a,c) and sketches (b,d) of Al single crystals used in this study with some of the facets slightly tilted from the (100) crystallographic plane. Reference vectors for the Al crystal lattice and tilting angles of the vicinal facets are also shown.

substrate on the AAO porous structure has been shown.^{20,21} In particular, the variation of transverse positional^{22,23} and transverse orientational²⁴ order in the structure of AAO film grown on metal grains with different crystallographic orientations has been experimentally observed. The best transverse positional order has been reported for Al(100) surfaces.^{22,23} On the contrary, the long-range transverse (in-plane) orientational correlations and the smallest mosaicity of the porous structure have been found for Al(111) substrates.²⁴

Here we compare the formation of AAO films on the low-index Al(100) surface with that on a number of vicinal facets. For the first time, the correlation between the longitudinal alignment and in-plane packing options of pores in anodic alumina films is demonstrated. Experiments on vicinal facets of single-crystal Al substrates allowed us to detect the deviation of the pore growth direction from the surface normal and to suggest the mechanism of inclination of channels.

EXPERIMENTAL METHODS

High-purity aluminum single crystals with (100) orientation (99.9999%, 2 mm thick, mechanically polished to a mirror finish) purchased from MESCREL²⁵ were used as starting material (Figure 1). Single crystal #1 has two areas tilted off the basal (100) plane by 1.9 and 4.1° around the [001] crystallographic direction. Single crystal #2 has three areas tilted off the basal (100) plane by ~5° around [001], [011], and [010] crystallographic directions. The tilt of vicinal facets was proved with an accuracy of 0.1° by reflection of laser beam ($\lambda \approx 650$ nm).

To obtain AAO film with ordered porous structure, we utilized two-step anodization in 0.3 M oxalic acid ($\text{H}_2\text{C}_2\text{O}_4$, 98%, Aldrich). The electrolyte was pumped through the two-electrode electrochemical cell using peristaltic pump Heidolph 5006, and its temperature was kept constant in the range of 1 to 2 °C by Huber K6 chiller. A constant voltage 40 V was applied using the Agilent N5751A DC power supply. Platinum wire was used as a counter electrode. Distance between electrodes was ~10 cm. The anodization area was restricted by a Viton O-ring with an internal diameter of 12 mm. The first anodization step was restricted by a charge limit of 105 C, which corresponds to AAO thickness of ca. 50 μm . After first anodization, alumina films were selectively etched away in an aqueous solution containing 0.5 M H_3PO_4 and 0.2 M CrO_3 at 70 °C for 30 min. Second anodization step was performed under the same conditions with a charge limit of 210 C. Thickness of the obtained AAO films was ca. 100 μm .

As a main tool for quantitative characterization of the ordering degree of AAO structure, high-resolution small-angle X-ray scattering (SAXS) was applied.^{26,27} SAXS is able to provide precise information on AAO porous structure including

the pore growth direction.²⁸ A scheme of the SAXS setup is presented in Figure 2.

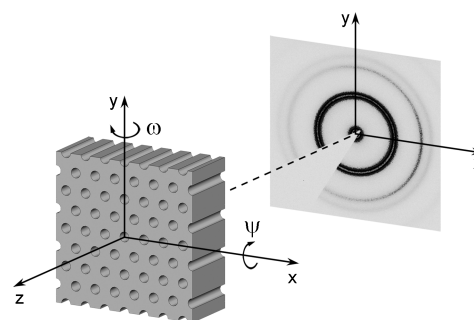


Figure 2. Scheme of the small-angle X-ray scattering setup. Rotation angles ω and ψ for vertical and horizontal axis orthogonal to the beam are shown.

Anodic alumina film was placed on the translation/rotation stage to allow careful orientation around the horizontal and vertical axes orthogonal to the beam and to collect data from the porous oxide film grown on different tilted zones. To minimize absorption of the transmitted X-ray beam, we partially dissolved the Al substrate in an aqueous solution of 0.5 M CuCl_2 and 1.4 M HCl at room temperature. The diffraction experiments were performed at the beamline BM26B “DUBBLE”²⁹ of the European Synchrotron Radiation Facility in Grenoble (France) using a microradian X-ray diffraction setup.^{30–32} A 13 keV X-ray beam (wavelength $\lambda = 0.95$ Å, bandpass $\Delta\lambda/\lambda = 2 \times 10^{-4}$, size 0.5×0.5 mm at the sample) was used. The beam was focused by a set of beryllium compound refractive lenses^{33,34} installed just in front of the sample. The lenses focused the beam at the phosphor screen of a 2D CCD detector (Photonic Science, 4008×2672 pixels of 22×22 μm). The detector was installed 7 m from the sample position.

Morphology characterization of the AAO porous films was carried out using a field-emission scanning electron microscope NVision 40 (Carl Zeiss). Pore ordering was analyzed from the bottom part of the oxide film after selective metal dissolution in a mixture of Br_2 and CH_3OH (1:10 vol.) at room temperature. Samples before SEM investigation were covered with a thin conductive layer of chromium using a Q150T ES sputter coater (Quorum Technologies).

Statistical analysis of SEM images was carried out via color-coding procedure proposed in ref 35. An average angle to the nearest neighbors of considered pore was measured. Taking account of a 6-fold symmetry, the average in-plane orientation of porous structure was reduced into a basic angle interval of $[0, 60^\circ]$ by adding or subtracting multiples of 60° . The horizontal direction is used as an anchoring azimuthal orientation. We

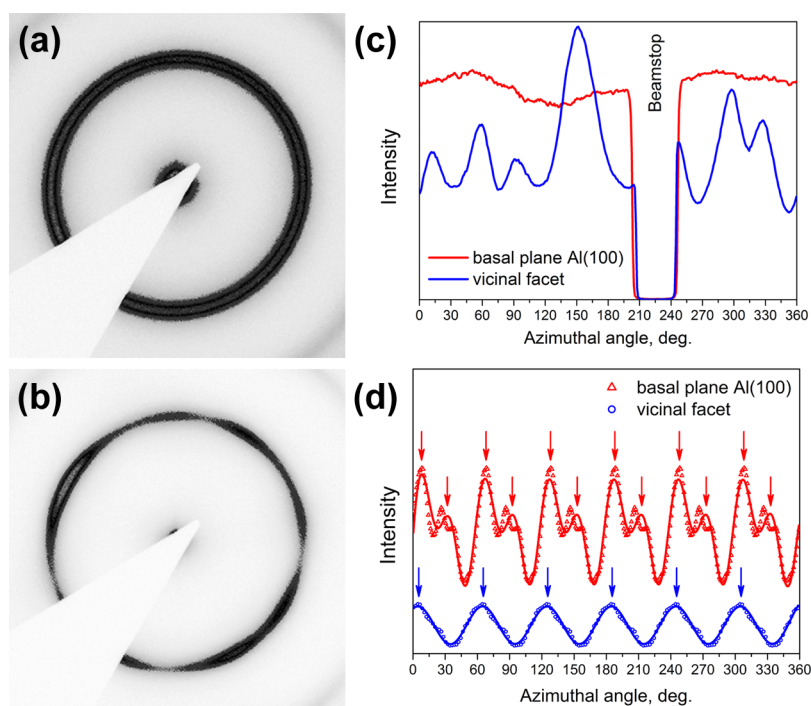


Figure 3. Small-angle diffraction patterns recorded at normal incidence of the X-ray beam to AAO film surface, grown on the Al(100) substrate (a) and on the vicinal facet of single crystal #1 tilted by 4.1° (b). The azimuthal profiles of the intensity for the first-order Bragg reflections (c). Transverse orientational correlations in AAO structure according to statistical analysis of scanning electron microscopy images (d). The solid lines in panel d show the results of a fit of the experimental data (open symbols) by a sum of Gauss functions. The arrows highlight the presence of 6-fold (vicinal surface) and 12-fold [Al(100)] modulation of the occurrence frequency.

should note that the above-mentioned procedure ignores point defects in AAO structure. As a consequence, only pores with a hexagonal coordination environment were included in calculations.

RESULTS AND DISCUSSION

According to small-angle diffraction patterns (Figure 3a,b) a small deviation of Al surface from the basal plane leads to significant changes in AAO porous structure. In the case of normal incidence of X-rays onto Al(100) basal plane a ring with uniform distribution of intensity is clearly observed, whereas for the vicinal facet the intensity is highly modulated along the ring (Figure 3c). The absence of preferred in-plane orientation of rows of pores in case of Al(100) substrate results from incompatibility of the 4-fold crystallographic symmetry of the underlying metal crystal and the hexagonal symmetry of the perfect AAO structure, which leads to the absolute equivalence of porous domains misoriented on 90° . Indeed, statistical orientation analysis^{24,35} of SEM images (Figure S1, Supporting Information) shows the presence of 12-fold modulation of the occurrence frequency with the intermaxima intervals of ca. 30° (Figure 3d), which confirms the presence of two preferential orientations of domains in AAO porous structure on Al(100).

On the vicinal facet the bimodal azimuthal distribution in each sextant changes to one broad maximum (Figure 3d). Thus, we can conclude that even a small deviation from the (100) orientation removes the equivalence of two stable in-plane orientations and, as a consequence, leads to an appearance of the preferred pore ordering direction. At the same time, diffraction patterns recorded for the AAO grown on vicinal facets cannot be interpreted as a diffraction from single domain region. They consist of more than six maxima with the

intermaxima distance in the azimuthal direction of ca. 30° but not of 60° , as one can expect for the hexagonal packing (Figure 3c). We stress that experimental diffraction pattern for oxide film grown on vicinal facet is noncentrosymmetric (Figure 3b,c). This feature appears due to the curvature of the Ewald sphere and was previously observed for perfect crystals of colloidal hard spheres,^{36,37} ion-track-etched polymer membranes,³⁸ ion tracks in natural minerals,³⁹ and anodic alumina porous films.^{26,28} We also note a substantial difference between the peak widths in the azimuthal distributions obtained from SEM and SAXS data for vicinal facet: 52.0 and 27.2° , respectively. To explain such an extraordinary behavior, we should address the directions of pore growth on Al(100) and vicinal facets.

The longitudinal orientational correlations in AAO structure were studied by measuring diffraction peak intensity as a function of sample orientation (rocking curve). Two sets of diffraction patterns were recorded during sample rotation around the vertical (ω scan) and horizontal (ψ scan) axis orthogonal to the beam (angles are introduced in Figure 2). The rocking curves for the intensity of 10 Bragg reflection (Figure 4) were obtained by averaging the radial distribution of the scattered intensity $I(q)$ inside the 60° sector of 2D SAXS patterns. Each point on the experimental curve represents the integral intensity of 10 diffraction peak obtained from the Lorentzian fit of $I(q)$ curve. For more details of rocking curve plotting, please refer to our recent paper.²⁶ The 10 Bragg reflections inside green and red sectors in Figure 4a were fitted during construction of the rocking curves for ψ and ω scans, respectively. The profiles of the rocking curves for AAO grown on the (100) plane of aluminum single crystal are typical for the system of the well-aligned channels—a narrow maximum with

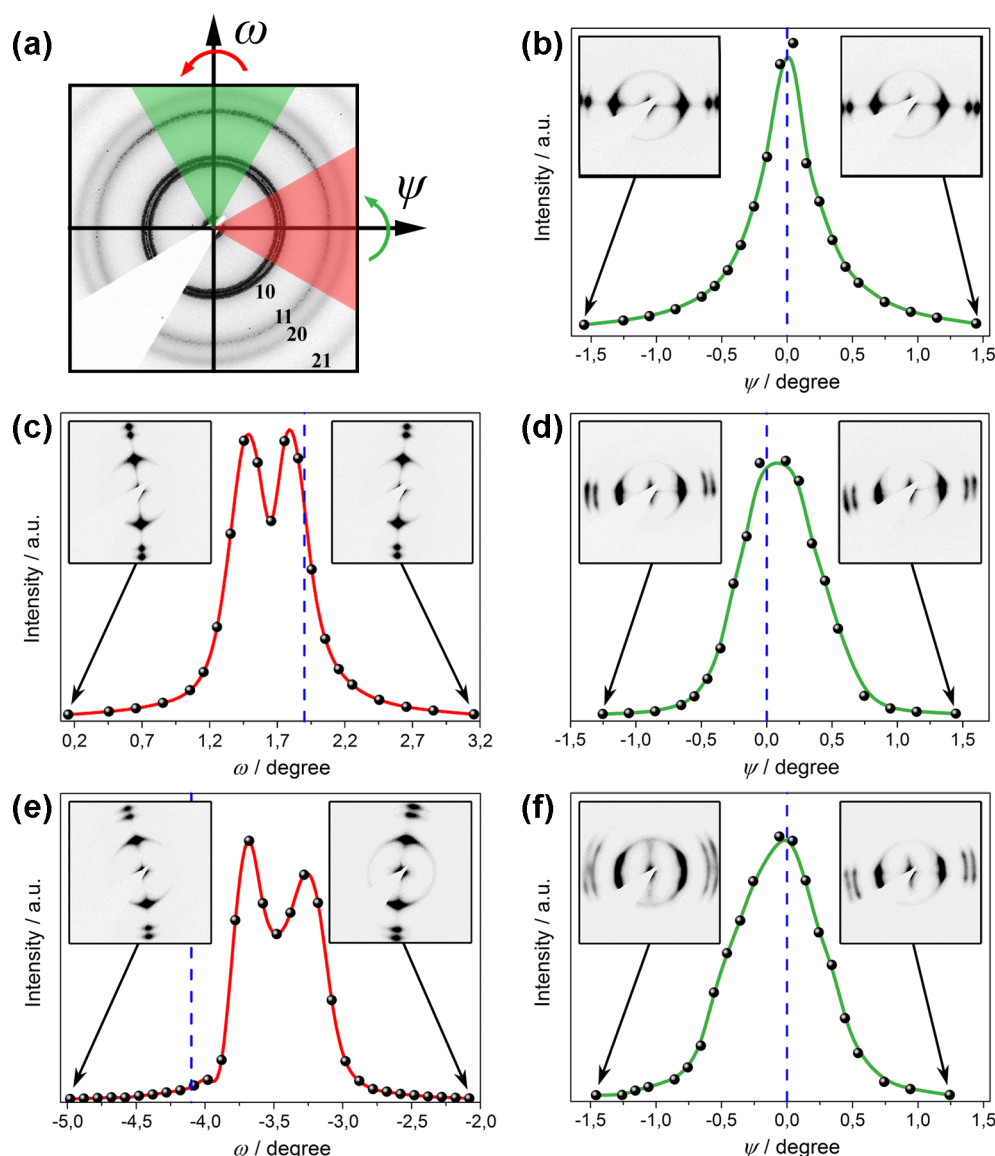


Figure 4. Small-angle diffraction pattern recorded at normal incidence of the X-ray beam to AAO film surface grown on the Al(100) single crystal #1 (a). *hk* indices for Bragg reflections are given. The green area indicates the 60° sector that was used to construct the ψ scans (b,d,f), whereas the area highlighted in red was used to generate the ω scans (c,e). Rocking curves for 10 Bragg reflections from the anodic oxide films grown on Al(100) (b) and on the vicinal facets of single crystal #1 with tilt angle of 1.9° (panels c and d) and 4.1° (panels e and f). ω scans (panels c and e) and ψ scans (panels b, d, and f) are obtained during sample rotation around vertical and horizontal axis orthogonal to the beam, respectively. All angles are given versus the surface normal of the basal aluminum plane with (100) orientation. The position of the normal to the single-crystal surface for each facet is denoted in both ω and ψ scales by blue dashed lines. The diffraction patterns for the highest rotation angles are shown in the insets.

a full width at half-maximum of $\sim 0.4^\circ$ and rapid intensity fall with the deviation from normal incidence of the X-ray beam to the AAO film surface (Figure 4b).

The rocking curves recorded for AAO on the vicinal facets look nothing like ψ and ω scans for oxide film on Al(100). In the case of porous structure on vicinal facets of the single crystal #1, two maxima on the ω scans are clearly observed (Figure 4c,e). They can be interpreted as the two preferential longitudinal orientations of the channels, which become parallel to the incident X-ray beam at different ω angles. Taking into account the single peak at $\psi = 0$ on ψ scan and the transformation of 2D diffraction patterns at the extreme values of ω into a set of point maxima on the vertical axis, we can conclude that aforementioned preferential longitudinal orientations of pores lie in the (001) plane. Thus, during AAO film

formation the direction of the growth of pores can vary slightly in (001) plane but cannot cross these highly symmetrical crystallographic planes. This assumption was proven by 2D diffraction patterns recorded during ψ scan: Twinned reflections are observed (inserts in Figure 4d,f) at extreme values of ψ .

Maxima positions on the rocking curves contain information about the preferential direction of the growth of pores. It is easy to see that the ψ -scan maxima position for the vicinal facets of the single crystal #1 are very close to zero (Figure 4d,f). On the contrary, two channel families in (001) crystallographic plane are significantly deviated from the orthogonal position to the film surface. Taking account of the tilting angles of the vicinal facets (Figure 1b), we can calculate the channels deviation angles from the normal growth direction. They were found to

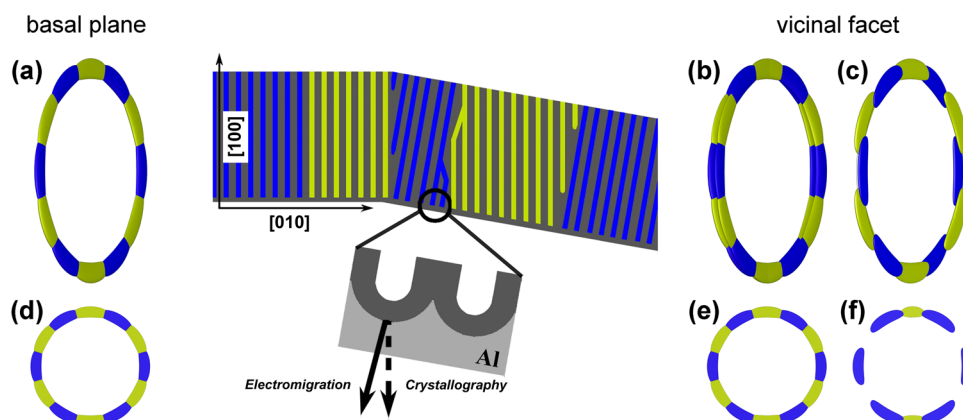


Figure 5. Scheme of the cross-section of AAO porous structure forming on the basal plane Al(100) and on vicinal facet (central panel). Channel families with different in-plane orientations are colored by different colors. Intensity distribution in 3D reciprocal space (a–c) and on 2D detector (d–f). In the case of porous structure on vicinal facet, two possible distributions of intensity corresponding to various structure organization are shown: (b,e) for random distribution of pores with various growth direction over domains or (c,f) for the case of strong correlation between the longitudinal alignment and in-plane packing options of pores in anodic alumina.

be equal to 0.09 and 0.44° for the green area (vicinal angle of 1.9°) and 0.46 and 0.89° for the blue-encoded part (vicinal angle of 4.1°), as can be observed in Figure 4c,e. It is clearly seen that for both vicinal facets the growth direction of one channel family is close to the normal to the corresponding facet, and the other channel family is deviated from normal to smaller ω angles. A similar effect of the deviation of pore growth direction on a small angle from surface normal was observed early for polycrystalline substrates.²⁸

The above-mentioned behavior is fully reproduced for the blue area of the single crystal #2 (Figure 1d). For the orange area it is also correct taking into account that the tilt direction is orthogonal to that in the blue region. The vicinal facet, which is colored violet in Figure 1d, shows the overlapping effect from blue and orange areas (for more details please refer to Figures S2 and S3, Supporting Information).

In general, one can consider two competing factors that can influence the growth direction of pores on the vicinal facets: (i) migration of the charged species under the external electric field in AAO barrier layer and (ii) anisotropy of anodic oxidation rate of the aluminum substrate (Figure 5, central panel). The first determines the growth of channels normal to the substrate. On the contrary, crossing of the stable crystallographic planes (010) and (001), which are perpendicular to the basal plane, by the pore is energetically unfavorable due to hampered transport of oxygen ions through dense atomic planes. This results in the inclination of the preferential direction of pore growth away from crystal planes with dense atomic packing.

Taking account of two in-plane packing options of porous domains and two preferable growth directions of channels in AAO on vicinal Al facet, we have plotted possible intensity distribution in 3D reciprocal space and the corresponding 2D diffraction pattern at nearly normal incidence of X-rays onto the film surface (Figure 5a–f). In the case of random distribution of pores with various growth directions over domains with two possible in-plane orientations, the intensity should concentrate into two uniform rings (Figure 5b), and in the diffraction experiment on the detector, we should observe uniform ring as well (Figure 5e). This prediction is far from the experimentally observed diffraction pattern (Figure 3b). Another option is the growth of pores forming hexagonal domains with various in-plane orientations in different longitudinal directions. In such a

case, two sets of diffraction maxima lying in intersecting planes should be observed in reciprocal space (Figure 5c). Simulated diffraction pattern (Figure 5f) exhibits eight maxima and is in good agreement with experimental data (Figure 3b).

It is worth noting that this kind of porous structure, where direction of pore growth depends on in-plane orientation of the domains, can explain the big difference in the azimuthal width of maxima obtained from SEM and SAXS techniques. In diffraction experiment, only channels family, which is parallel to the incident X-ray beam, gives six-fold SAXS pattern. Thus, mosaicity obtained by SAXS is related to the spread of in-plane orientations of one of two sorts of domains, while SEM method is not sensitive to pore growth direction and consequently provides us averaged orientations of all domains. For vicinal facets the azimuthal width of diffraction peaks is very close to the one, which was previously observed for AAO films within single grain of the polycrystalline Al substrates by SAXS²⁶ and SEM²⁴ techniques.

CONCLUSIONS

Our experimental findings suggest the presence of a strong correlation between transverse and longitudinal orientational pore ordering in porous anodic films grown on aluminum substrates. It has been shown that domains in porous structure with different in-plane orientation contain the channels possessing different growth direction.

The use of single-crystal Al(100) substrates with a number of vicinal surfaces allowed us to study the transformation of AAO porous structure with equivalent in-plane orientations of domains misoriented by 90° to the structure with long-range transverse orientational ordering, where the certain in-plane packing option becomes preferable. The porous structure formed on vicinal facets exhibits a coexistence of two direction of pores growth with the disorientation angle of $\sim 0.4^\circ$. This duality appears owing to the competitive impact of the electromigration driving force and the anisotropic behavior of crystal substrate with the primary role of first one. Deviation from the normal direction originated by the influence of the substrate crystal structure does not exceed 1° .

Our findings provide a new insight into the anodization of textured Al foils and potentially of any valve metals, which are widely used in industry.

■ ASSOCIATED CONTENT

■ Supporting Information

The Supporting Information is available free of charge on the ACS Publications website at DOI: 10.1021/acs.jpcc.6b05268.

SEM images and color-coded patterns of anodic alumina films, small-angle diffraction patterns, and rocking curves. (PDF)

■ AUTHOR INFORMATION

Corresponding Author

*E-mail: napolsky@inorg.chem.msu.ru. Phone: +7-916-2323829. Fax: +7-495-9390998.

Notes

The authors declare no competing financial interest.

■ ACKNOWLEDGMENTS

The work is supported by Russian Science Foundation (Grant No. 14-13-00809). We thank the personnel of the DUBBLE beamline for their excellent support during experiments. The Nederlandse Organisatie voor Wetenschappelijk Onderzoek is thanked for granting the beam time.

■ REFERENCES

- (1) Masuda, H.; Satoh, M. Fabrication of Gold Nanodot Array Using Anodic Porous Alumina as an Evaporation Mask. *Jpn. J. Appl. Phys.* **1996**, *35*, L126–L129.
- (2) Lee, W.; Ji, R.; Gosele, U.; Nielsch, K. Fast Fabrication of Long-Range Ordered Porous Alumina Membranes by Hard Anodization. *Nat. Mater.* **2006**, *5*, 741–747.
- (3) Lau, K. H. A.; Tan, L. S.; Tamada, K.; Sander, M. S.; Knoll, W. Highly Sensitive Detection of Processes Occurring Inside Nanoporous Anodic Alumina Templates: A Waveguide Optical Study. *J. Phys. Chem. B* **2004**, *108*, 10812–10818.
- (4) Apolinario, A.; Quiterio, P.; Sousa, C. T.; Ventura, J.; Sousa, J. B.; Andrade, L.; Mendes, A. M.; Araujo, J. P. Modeling the Growth Kinetics of Anodic TiO₂ Nanotubes. *J. Phys. Chem. Lett.* **2015**, *6*, 845–851.
- (5) Guo, Z.; Prezhdov, O. V.; Hou, T.; Chen, X.; Lee, S. T.; Li, Y. Fast Energy Relaxation by Trap States Decreases Electron Mobility in TiO₂ Nanotubes: Time-Domain Ab Initio Analysis. *J. Phys. Chem. Lett.* **2014**, *5*, 1642–1647.
- (6) de Tacconi, N. R.; Chenthamarakshan, C. R.; Yogeewaran, G.; Watcharenwong, A.; de Zoysa, R. S.; Basit, N. A.; Rajeshwar, K. Nanoporous TiO₂ and WO₃ Films by Anodization of Titanium and Tungsten Substrates: Influence of Process Variables on Morphology and Photoelectrochemical Response. *J. Phys. Chem. B* **2006**, *110*, 25347–25355.
- (7) Petukhov, D. I.; Eliseev, A. A.; Kolesnik, I. V.; Napolskii, K. S.; Lukashin, A. V.; Tretyakov, Y. D.; Grigoriev, S. V.; Grigorieva, N. A.; Eckerlebe, H. Formation Mechanism and Packing Options in Tubular Anodic Titania Films. *Microporous Mesoporous Mater.* **2008**, *114*, 440–447.
- (8) Fang, D.; Huang, K.; Luo, Z.; Wang, Y.; Liu, S.; Zhang, Q. Freestanding ZrO₂ Nanotube Membranes Made by Anodic Oxidation and Effect of Heat Treatment on Their Morphology and Crystalline Structure. *J. Mater. Chem.* **2011**, *21*, 4989–4994.
- (9) Tsuchiya, H.; Macak, J. M.; Taveira, L.; Schmuki, P. Fabrication and Characterization of Smooth High Aspect Ratio Zirconia Nanotubes. *Chem. Phys. Lett.* **2005**, *410*, 188–191.
- (10) Ng, C.; Iwase, A.; Ng, Y. H.; Amal, R. Transforming Anodized WO₃ Films into Visible-Light-Active Bi₂WO₆ Photoelectrodes by Hydrothermal Treatment. *J. Phys. Chem. Lett.* **2012**, *3*, 913–918.
- (11) Mikulskas, I.; Juodkazis, S.; Tomasiunas, R.; Dumas, J. G. Aluminum Oxide Photonic Crystals Grown by a New Hybrid Method. *Adv. Mater. (Weinheim, Ger.)* **2001**, *13*, 1574–1577.
- (12) Kikuchi, T.; Nishinaga, O.; Natsui, S.; Suzuki, R. O. Fabrication of Self-Ordered Porous Alumina via Etidronic Acid Anodizing and Structural Color Generation from Submicrometer-Scale Dimple Array. *Electrochim. Acta* **2015**, *156*, 235–243.
- (13) Petukhov, D. I.; Eliseev, A. A. Gas Permeation through Nanoporous Membranes in the Transitional Flow Region. *Nanotechnology* **2016**, *27*, 085707.
- (14) Petukhov, D. I.; Napolskii, K. S.; Eliseev, A. A. Permeability of Anodic Alumina Membranes with Branched Channels. *Nanotechnology* **2012**, *23*, 335601.
- (15) Tsou, P. H.; Sreenivasappa, H.; Hong, S.; Yasuie, M.; Miyamoto, H.; Nakano, K.; Misawa, T.; Kameoka, J. Rapid Antibiotic Efficacy Screening with Aluminum Oxide Nanoporous Membrane Filter-Chip and Optical Detection System. *Biosens. Bioelectron.* **2010**, *26*, 289–294.
- (16) Chumakov, A. P.; Grigoriev, S. V.; Grigoryeva, N. A.; Napolskii, K. S.; Eliseev, A. A.; Roslyakov, I. V.; Okorokov, A. I.; Eckerlebe, H. Magnetic Properties of Cobalt Nanowires: Study by Polarized SANS. *Phys. B (Amsterdam, Neth.)* **2011**, *406*, 2405–2408.
- (17) Lukatskaya, M. R.; Trusov, L. A.; Eliseev, A. A.; Lukashin, A. V.; Jansen, M.; Kazin, P. E.; Napolskii, K. S. Controlled Way to Prepare Quasi-1D Nanostructures with Complex Chemical Composition in Porous Anodic Alumina. *Chem. Commun. (Cambridge, U. K.)* **2011**, *47*, 2396–2398.
- (18) Zong, R. L.; Zhou, J.; Li, Q.; Du, B.; Li, B.; Fu, M.; Qi, X. W.; Li, L. T.; Buddhudu, S. Synthesis and Optical Properties of Silver Nanowire Arrays Embedded in Anodic Alumina Membrane. *J. Phys. Chem. B* **2004**, *108*, 16713–16716.
- (19) Lee, W.; Park, S. J. Porous Anodic Aluminum Oxide: Anodization and Templated Synthesis of Functional Nanostructures. *Chem. Rev. (Washington, DC, U. S.)* **2014**, *114*, 7487–7556.
- (20) Grigoriev, S. V.; Grigorieva, N. A.; Syromyatnikova, A. V.; Napolskii, K. S.; Eliseev, A. A.; Lukashin, A. V.; Tretyakov, Y. D.; Eckerlebe, H. Two-Dimensional Spatially Ordered Al₂O₃ Systems: Small-Angle Neutron Scattering Investigation. *JETP Lett.* **2007**, *85*, 449–453.
- (21) Beck, G.; Petrikowski, K. Influence of the Microstructure of the Aluminum Substrate on the Regularity of the Nanopore Arrangement in an Alumina Layer Formed by Anodic Oxidation. *Surf. Coat. Technol.* **2008**, *202*, 5084–5091.
- (22) Beck, G.; Bretzler, R. Regularity of Nanopores in Anodic Alumina Formed on Orientated Aluminium Single-Crystals. *Mater. Chem. Phys.* **2011**, *128*, 383–387.
- (23) Ng, C. K. Y.; Ngan, A. H. W. Precise Control of Nanohoneycomb Ordering over Anodic Aluminum Oxide of Square Centimeter Areas. *Chem. Mater.* **2011**, *23*, 5264–5268.
- (24) Napolskii, K. S.; Roslyakov, I. V.; Romanchuk, A. Y.; Kapitanova, O. O.; Mankevich, A. S.; Lebedev, V. A.; Eliseev, A. A. Origin of Long-Range Orientational Pore Ordering in Anodic Films on Aluminium. *J. Mater. Chem.* **2012**, *22*, 11922–11926.
- (25) Mescrel: Metal Single Crystals, Single Crystal Electrodes and Substrates. www.mescrel.com.
- (26) Napolskii, K. S.; Roslyakov, I. V.; Eliseev, A. A.; Petukhov, A. V.; Byelov, D. V.; Grigoryeva, N. A.; Bouwman, W. G.; Lukashin, A. V.; Kvashnina, K. O.; Chumakov, A. P.; et al. Long-Range Ordering in Anodic Alumina Films: A Microradian X-ray Diffraction Study. *J. Appl. Crystallogr.* **2010**, *43*, 531–538.
- (27) Napolskii, K. S.; Roslyakov, I. V.; Eliseev, A. A.; Byelov, D. V.; Petukhov, A. V.; Grigoryeva, N. A.; Bouwman, W. G.; Lukashin, A. V.; Chumakov, A. P.; Grigoriev, S. V. The Kinetics and Mechanism of Long-Range Pore Ordering in Anodic Films on Aluminium. *J. Phys. Chem. C* **2011**, *115*, 23726–23731.
- (28) Roslyakov, I. V.; Eliseev, A. A.; Yakovenko, E. V.; Zabelin, A. V.; Napolskii, K. S. Longitudinal Pore Alignment in Anodic Alumina Films Grown on Polycrystalline Metal Substrates. *J. Appl. Crystallogr.* **2013**, *46*, 1705–1710.
- (29) Bras, W.; Dolbnya, I. P.; Detollenaere, D.; van Tol, R.; Malfois, M.; Greaves, G. N.; Ryan, A. J.; Heeley, E. Recent Experiments on a

Small-Angle/Wide-Angle X-ray Scattering Beam Line at the ESRF. *J. Appl. Crystallogr.* **2003**, *36*, 791–794.

(30) Petukhov, A. V.; Thijssen, J. H. J.; 't Hart, D. C.; Imhof, A.; van Blaaderen, A.; Dolbnya, I. P.; Snigirev, A.; Moussaid, A.; Snigireva, I. Microradian X-ray Diffraction in Colloidal Photonic Crystals. *J. Appl. Crystallogr.* **2006**, *39*, 137–144.

(31) Thijssen, J. H. J.; Petukhov, A. V.; 't Hart, D. C.; Imhof, A.; van der Werf, C. H.; Schropp, R. E.; van Blaaderen, A. Characterization of Photonic Colloidal Single Crystals by Microradian X-ray Diffraction. *Adv. Mater. (Weinheim, Ger.)* **2006**, *18*, 1662–1666.

(32) Petukhov, A. V.; Meijer, J. M.; Vroege, G. J. Particle Shape Effects in Colloidal Crystals and Colloidal Liquid Crystals: Small-Angle X-ray Scattering Studies with Microradian Resolution. *Curr. Opin. Colloid Interface Sci.* **2015**, *20*, 272–281.

(33) Snigirev, A.; Kohn, V.; Snigireva, I.; Lengeler, B. A Compound Refractive Lens for Focusing High-Energy X-rays. *Nature (London, U. K.)* **1996**, *384*, 49–51.

(34) Bosak, A.; Snigireva, I.; Napolskii, K. S.; Snigirev, A. High-Resolution Transmission X-ray Microscopy: A New Tool for Mesoscopic Materials. *Adv. Mater. (Weinheim, Ger.)* **2010**, *22*, 3256–3259.

(35) Hillebrand, R.; Muller, F.; Schwirn, K.; Lee, W.; Steinhart, M. Quantitative Analysis of the Grain Morphology in Self-Assembled Hexagonal Lattices. *ACS Nano* **2008**, *2*, 913–920.

(36) Petukhov, A. V.; Aarts, D. G. A. L.; Dolbnya, I. P.; de Hoog, E. H. A.; Kassapidou, K.; Vroege, G. J.; Bras, W.; Lekkerkerker, H. N.W. High-Resolution Small-Angle X-ray Diffraction Study of Long-Range Order in Hard-Sphere Colloidal Crystals. *Phys. Rev. Lett.* **2002**, *88*, 208301.

(37) Petukhov, A. V.; Dolbnya, I. P.; Aarts, D. G. A. L.; Vroege, G. J. Destruction of Long-Range Order Recorded with In Situ Small-Angle X-ray Diffraction in Drying Colloidal Crystals. *Phys. Rev. E* **2004**, *69*, 031405.

(38) Engel, M.; Stuhn, B.; Schneider, J. J.; Cornelius, T.; Naumann, M. Small-Angle X-ray Scattering (SAXS) off Parallel, Cylindrical, Well-Defined Nanopores: from Random Pore Distribution to Highly Ordered Samples. *Appl. Phys. A: Mater. Sci. Process.* **2009**, *97*, 99–108.

(39) Afra, B.; Lang, M.; Rodriguez, M. D.; Zhang, J.; Giulian, R.; Kirby, N.; Ewing, R. C.; Trautmann, C.; Toulemonde, M.; Kluth, P. Annealing Kinetics of Latent Particle Tracks in Durango Apatite. *Phys. Rev. B: Condens. Matter Mater. Phys.* **2011**, *83*, 064116.